

UC Santa Barbara

UC Santa Barbara Previously Published Works

Title

Effect of extended defects on photoluminescence of gallium oxide and aluminum gallium oxide epitaxial films

Permalink

<https://escholarship.org/uc/item/20w8s16k>

Journal

Scientific Reports, 12(1)

ISSN

2045-2322

Authors

Cooke, Jacqueline

Ranga, Praneeth

Jesenovec, Jani

et al.

Publication Date

2022

DOI

10.1038/s41598-022-07242-z

Copyright Information

This work is made available under the terms of a Creative Commons Attribution License, available at <https://creativecommons.org/licenses/by/4.0/>

Peer reviewed



OPEN

Effect of extended defects on photoluminescence of gallium oxide and aluminum gallium oxide epitaxial films

Jacqueline Cooke¹, Praneeth Ranga¹, Jani Jesenovc^{4,5}, John S. McCloy^{4,5},
Sriram Krishnamoorthy³, Michael A. Scarpulla^{1,2} & Berardi Sensale-Rodriguez¹✉

In this work, a systematic photoluminescence (PL) study on three series of gallium oxide/aluminum gallium oxide films and bulk single crystals is performed including comparing doping, epitaxial substrates, and aluminum concentration. It is observed that blue/green emission intensity strongly correlates with extended structural defects rather than the point defects frequently assumed. Bulk crystals or Si-doped films homoepitaxially grown on (010) β -Ga₂O₃ yield an intense dominant UV emission, while samples with extended structural defects, such as gallium oxide films grown on either (-201) β -Ga₂O₃ or sapphire, as well as thick aluminum gallium oxide films grown on either (010) β -Ga₂O₃ or sapphire, all show a very broad PL spectrum with intense dominant blue/green emission. PL differences between samples and the possible causes of these differences are analyzed. This work expands previous reports that have so far attributed blue and green emissions to point defects and shows that in the case of thin films, extended defects might have a prominent role in emission properties.

Gallium oxide is an ultra-wide bandgap semiconductor, with its most thermally and chemically stable phase being the monoclinic structure, β -Ga₂O₃. It has an indirect, fundamental bandgap near 276 nm (4.5 eV) though optical transition energies range from 282 to 253 nm (4.5 to 4.9 eV) depending on the crystallographic orientation due to the anisotropy of this material¹. β -Ga₂O₃ has a large Baliga's figure of merit which has increasingly garnered interest in various electronics and optoelectronics applications. Understanding and characterizing the material properties, including its defects, has been a priority, and photoluminescence (PL) has been under intense scrutiny in an attempt to define the mechanisms that generate the emissions in this material.

In general, PL spectra can be used to characterize the defects leading to radiative recombination processes within a specific material. In this regard, the PL spectra for β -Ga₂O₃ has generally been deconvoluted in three emission peaks: UV, blue, and green. However, it is notable that peak shapes from any point defect are expected to require more than a single Gaussian for a complex crystal structure like β -Ga₂O₃, possibly having an asymmetric shape and requiring a more complex model such as Huang-Rhys or Franck-Condon, which takes into consideration the vibrational broadening of the PL spectrum caused by electron-phonon coupling²⁻⁴. The sum of so many phonon replicas makes it challenging to fit the spectra uniquely. Adding energy level broadening from disorder or extended defects makes the deconvolution of the β -Ga₂O₃ PL spectra even more difficult. As such, in β -Ga₂O₃ with strong electron phonon coupling, there is little chance of being able to spectroscopically discern different types of defects from luminescence as any defect considered can result in a very wide luminescence band, even near 0 Kelvin. This has resulted in an intense debate in defining the defects and phenomenological explanations of electronic processes that cause these particular emissions⁵⁻²⁴. Provided in the Supplementary Information is a comprehensive review of the literature.

Point defects have been the only explored and discussed potential source for the visible PL emission peaks in β -Ga₂O₃. Generally, there has been recent agreement on an intrinsic origin of UV luminescence and an

¹Department of Electrical and Computer Engineering, The University of Utah, Salt Lake City, UT 84112, USA. ²Department of Materials Science and Engineering, The University of Utah, Salt Lake City, UT 84112, USA. ³Materials Department, University of California, Santa Barbara, Santa Barbara, CA 93106-5050, USA. ⁴Institute of Materials Research, Washington State University, Pullman, WA 99164-2920, USA. ⁵Materials Science and Engineering Program, Washington State University, Pullman, WA 99164, USA. ✉email: berardi.sensale@utah.edu

| Samples | Doping (cm ⁻³) | Dopant | Orientation | Substrate | Film or crystal thickness (μm) | Growth temp. (°C) | TEGa flow rate (sccm) | TMAI molar ratio (push/purge/double dilution) |
|--|----------------------------|----------|-------------|---|--------------------------------|---|-----------------------|---|
| Si series | | | | | | | | |
| UID β-Ga ₂ O ₃ | 3 × 10 ¹⁶ | Si (UID) | (010) | Fe-doped β-Ga ₂ O ₃ | 1 | 600 | 65 | |
| β-doped Ga ₂ O ₃ | 1.5 × 10 ¹⁷ | Si | (010) | Fe-doped β-Ga ₂ O ₃ | 1 | 600 | 65 | |
| Heavy doped β-Ga ₂ O ₃ | 5 × 10 ¹⁸ | Si | (010) | Fe-doped β-Ga ₂ O ₃ | 1 | 600 | 65 | |
| (-201) oriented series | | | | | | | | |
| Bulk β-Ga ₂ O ₃ | 1.9 × 10 ¹⁷ | UID | (-201) | Bulk | 670 | Purchased from Novel Crystal Technology (EFG method) | | |
| β-Ga ₂ O ₃ on β-Ga ₂ O ₃ | ~ 10 ¹⁶ | UID | (-201) | Fe-doped β-Ga ₂ O ₃ | 0.350–0.400 | 650 | 65 | |
| β-Ga ₂ O ₃ on sapphire | ~ 10 ¹⁶ | UID | (-201) | Sapphire | ~ 0.400 | 810 | 65 | |
| Samples | % Concentration | Dopant | Orientation | Substrate | Film or crystal thickness (μm) | Growth temp. (°C) | TEGa flow rate (sccm) | TMAI molar ratio (push/purge/double dilution) |
| AGO series | | | | | | | | |
| β-Ga ₂ O ₃ on β-Ga ₂ O ₃ | | UID | (010) | Fe-doped β-Ga ₂ O ₃ | 0.350–0.400 | 650 | 65 | |
| 10% AGO on β-Ga ₂ O ₃ | 10 (PMR) | Al | (010) | Fe-doped β-Ga ₂ O ₃ | 0.350–0.400 | 650 | 58.5 | 10/200/84 |
| 25% AGO on β-Ga ₂ O ₃ | 25 (EDS) | Al | (010) | Fe-doped β-Ga ₂ O ₃ | 0.350–0.400 | 650 | 52 | 15/100/1.5 |
| 10% bulk AGO | 10 (XRF) | Al | (100) | Bulk | ~ 2000 | From Washington State University (Czochralski method) | | |
| β-Ga ₂ O ₃ on sapphire | | UID | (-201) | Sapphire | ~ 0.400 | 810 | 65 | |
| 2% AGO on Sapphire | 2 (XRD) | Al | (-201) | Sapphire | ~ 0.400 | 810 | 61.6 | 10/200/42 |
| 10% AGO on Sapphire | 10 (XRD) | Al | (-201) | Sapphire | ~ 0.400 | 810 | 58.5 | 10/150/64 |
| 28% AGO on Sapphire | 28 (XRD) | Al | (-201) | Sapphire | ~ 0.400 | 810 | 48.7 | 30/100/43.5 |

Table 1. Growth parameters for all the analyzed samples.

extrinsic origin of visible emission. But, as far as can be determined, no previous works in the literature have discussed whether extended defects affect PL. Here, by systematically analyzing a series of thin-film samples, it is observed that extended defects substantially affect blue/green emissions and that this is correlated with poor structural quality samples. This analysis expands on previous reports that have so far attributed blue and green emissions to point defects and shows that in the case of thin films, extended defects may have a prominent role in emission properties.

Experiment

Sample preparation. All film samples were grown using metal–organic vapor-phase epitaxy (MOVPE) in an Agnition Agilis reactor. All samples were grown using triethylgallium (TEGa) and O₂ as the gallium and oxygen precursors, respectively, and silane as the Si dopant source when applicable. Growth details are listed in Table 1. Parameters used for all samples include a total molar flow of 15.53 μmol/min, argon flow rate of 1100 sccm, an oxygen flow rate of 500 sccm, and a chamber pressure of 15 Torr with a growth rate of around 6 nm/min. The substrates used for growth were either Fe-doped (-201) or (010) oriented β-Ga₂O₃ grown by Novel Crystal Technology. Otherwise, C-plane sapphire was used for growth and purchased from Cryscore. An unintentionally doped (UID) single crystal (-201) oriented β-Ga₂O₃ bulk sample grown using edge-defined film fed (EFG) technology was purchased from Novel Crystal Technology. Lastly, a single crystal (100) oriented 10% bulk aluminum-gallium oxide (AGO) sample, β-Al_{0.2}Ga_{1.8}O₃ was grown using the Czochralski method. Details on the bulk AGO sample and growth can be found in²⁵.

Three series of samples were analyzed. The first series includes three film samples with varying Si-doping (used to make β-Ga₂O₃ more conductive and due to its strong PL signature): UID (~ 10¹⁶ cm⁻³), ~ 10¹⁷ cm⁻³, and ~ 10¹⁸ cm⁻³, with required silane flows determined using silicon secondary ion mass spectrometry (SIMS) calibrations²⁶. All samples in the series are (010) oriented Si-doped β-Ga₂O₃ film grown on Fe-doped β-Ga₂O₃. The second series also contains three samples and compares (-201) β-Ga₂O₃. This series includes a bulk crystal of (-201) UID β-Ga₂O₃, a (-201) UID β-Ga₂O₃ film grown on Fe-doped β-Ga₂O₃, and a (-201) UID β-Ga₂O₃ film grown on sapphire. The last series compares (010) oriented (Al_xGa_{1-x})₂O₃ films, i.e., AGO of varying Al concentrations, grown on Fe-doped β-Ga₂O₃. These are compared to a (100) oriented bulk 10% AGO (β-Al_{0.2}Ga_{1.8}O₃) crystal. The second half of the series compares (-201) oriented 0%, 2%, 10%, and 28% AGO films grown on sapphire.

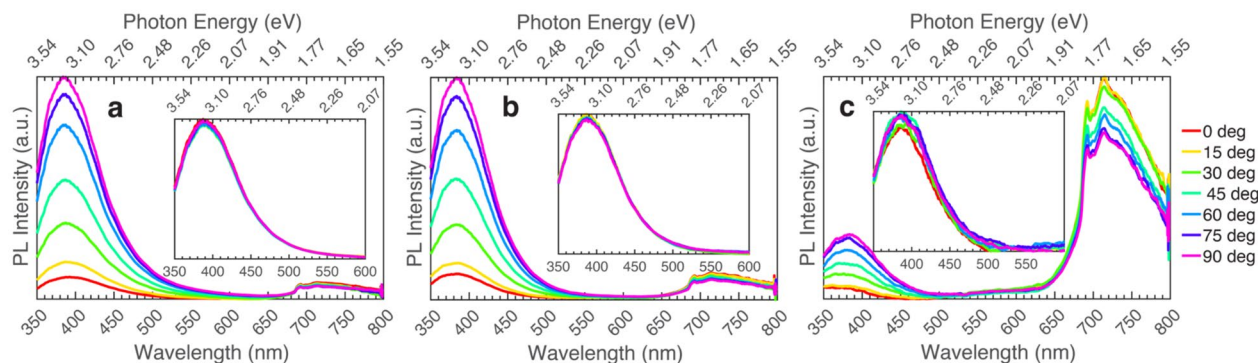


Figure 1. Polarized photoluminescence of β -Ga₂O₃ grown on (010) Fe-doped β -Ga₂O₃ excited at 267 nm (4.64 eV). Insets show data for the same samples but excited at 235 nm (5.27 eV). **(a)** UID ($\sim 10^{16} \text{ cm}^{-3}$) β -Ga₂O₃ grown on (010) Fe-doped β -Ga₂O₃, **(b)** Si-doped ($1.5 \times 10^{17} \text{ cm}^{-3}$) β -Ga₂O₃ grown on (010) Fe-doped β -Ga₂O₃, **(c)** Si-doped ($5 \times 10^{18} \text{ cm}^{-3}$) β -Ga₂O₃ grown on (010) Fe-doped β -Ga₂O₃.

X-ray diffraction (XRD) was performed on all epitaxial AGO films. For AGO films grown on sapphire, the value obtained from XRD is used to define the aluminum concentration. Note that the AGO samples grown on Fe-doped β -Ga₂O₃ yielded Al composition values that were much larger than expected: 20% for the nominally 10% AGO sample (i.e., grown using a molar ratio that should have yielded $\sim 10\%$ Al) and 30% for the nominally 25% AGO sample (i.e., grown using a molar ratio that should have produced $\sim 20\%$ Al). This is likely due to strain and relaxation that occurs in the homoepitaxial film, which was found riddled with extended defects using STEM (shown in the results section). Furthermore, EDS measurements verified an aluminum concentration of 25% for the nominal 25% AGO sample. Therefore, for the 10% AGO sample, an Al composition value from the precursor molar ratio (PMR) during growth is used instead of the value obtained from XRD. The bulk AGO sample was measured by Washington State University using X-ray fluorescence (XRF) and found to have an Al composition of 10%²⁵.

Characterization. Photoluminescence was performed using ultrafast (fs) pulses from a wavelength-tunable (690–1040 nm or 1.8–1.2 eV) Ti:Sapphire (Coherent Chameleon Vision Ultra) laser, which passed through a third-harmonic generator (Coherent Harmonics). The laser was then polarized using a linear polarizer (Glan-Laser alpha-BBO polarizer prism, 210–450 nm or 5.9–2.76 eV) followed by a zero-order half-wave plate to control the polarization angle of the laser. The laser excited the sample at normal incidence within an integration sphere. The PL spectra were collected at room temperature using an optical fiber connected to a broadband spectrometer in the range of 300–800 nm or 4.13–1.55 eV (Avasoft AvaSpec dual-channel spectrometer).

Samples were measured using an excitation of 235 nm (5.27 eV) (236 nm or 5.25 eV for AGO grown on sapphire), 254 nm (4.88 eV), and 267 nm (4.64 eV). Polarization was altered from 0 to 180 degrees with a 15-degree step size. The collected data was corrected to remove the response caused by the spectrometer and eliminate the grating and detector response, so as to extract the response of the sample itself. The data collected was corrected for the spectrometer spectra using the Ocean Insight HL-3 plus visible-near infrared (VIS–NIR) light source. The spectrum for this light source was calibrated by Shanghai Calibration Laboratory. The calibrated blackbody radiant energy spectra from the laboratory was divided by the spectra collected by our spectrometer to get a correction factor. This correction factor was then applied to the spectra collected for all samples except AGO samples grown on sapphire. The AGO samples grown on sapphire used a quartz-tungsten-halogen (QTH) lamp (Oriental Instruments), whose spectrum is well defined as a blackbody source given by Planck's radiation law. The measured light source was fitted to this radiation law, and a temperature correction factor was applied for the corrected data. These correction factors were then applied to measured PL data for the AGO samples grown on sapphire. All the corrected spectra were then normalized by the power measured (using a Newport optical power meter 1830-C) and integration time (which was kept at 5 s for all samples).

Results

Si series. Depicted in Fig. 1 is the measured polarized PL for all the samples in the series excited above and below the bandgap. Panels (a–c) correspond to the polarized emission spectrum of each sample: UID ($\sim 10^{16} \text{ cm}^{-3}$) β -Ga₂O₃ grown on Fe-doped (010) oriented β -Ga₂O₃ substrate, Si-doped ($1.5 \times 10^{17} \text{ cm}^{-3}$) β -Ga₂O₃ grown on Fe-doped (010) oriented β -Ga₂O₃ substrate, and Si-doped ($5 \times 10^{18} \text{ cm}^{-3}$) β -Ga₂O₃ grown on Fe-doped (010) oriented β -Ga₂O₃ substrate. For the main plots in each panel, an excitation wavelength of 267 nm (4.64 eV) is employed, whereas the insets correspond to 235 nm (5.27 eV) excitation wavelength. All three samples in the Si series show a dominant UV emission, with peak emission around 385 nm (3.22 eV) for excitation both below (267 nm or 4.64 eV) and above (235 nm or 5.27 eV) bandgap. Polarization dependence of emission is seen below the bandgap for all three samples. The observed red emission starting around 700 nm (1.77 eV) is due to the Fe-doped β -Ga₂O₃ substrate on which the Si-doped β -Ga₂O₃ films were grown^{27,28}.

The PL of the varying Si-doped samples grown on Fe-doped β -Ga₂O₃ is compared in Fig. 2, excited above and below the bandgap. This series of samples revealed that increasing Si doping leads to a decrease in overall PL

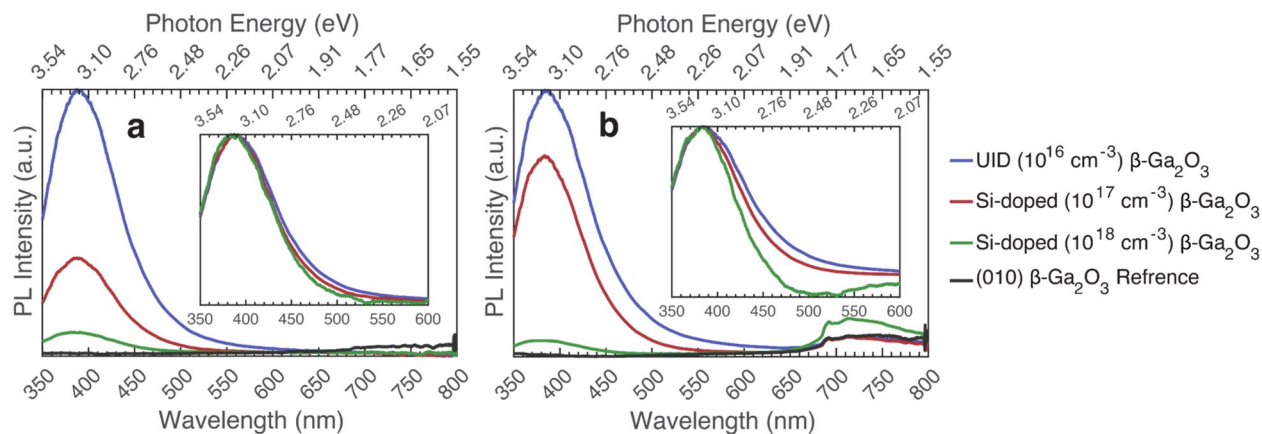


Figure 2. Photoluminescence comparison (taken at max polarization) of Si-doped β -Ga₂O₃ series grown on (010) Fe-doped β -Ga₂O₃. Insets show the same data but normalized to peak intensity. (a) Excited at 235 nm (5.27 eV), (b) Excited at 267 nm (4.64 eV).

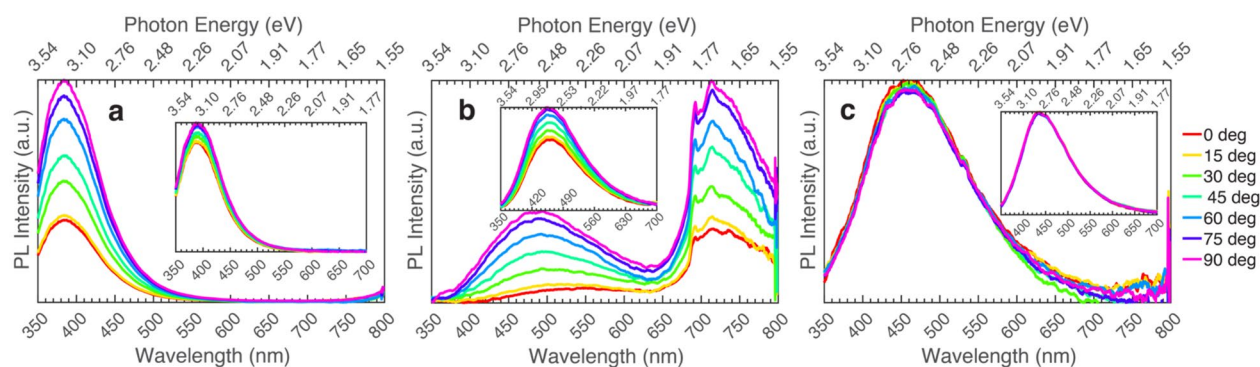


Figure 3. Polarized photoluminescence of β -Ga₂O₃ grown on different substrates excited at 267 nm (4.64 eV). Insets show data for the same samples but excited at 235 nm (5.27 eV). (a) Bulk (-201) β -Ga₂O₃, (b) β -Ga₂O₃ grown on (-201) Fe-doped β -Ga₂O₃, (c) (-201) β -Ga₂O₃ grown on c-plane sapphire.

intensity. This is likely due to an increase in non-radiative recombination^{7,13,29}. The dominant emission within the UV region (385 nm or 3.22 eV) does not change between the samples. This is possibly due to the samples having a homogeneous film with limited extended defects. Transmission electron microscopy (TEM) images in previous reports show that β -Ga₂O₃ films grown on (010) β -Ga₂O₃ continue to have the same crystal structure as the substrate, with no stacking faults or other extended defects^{30,31}. However, there is a decrease in the blue luminescence (from 400 to 500 nm or 3.1 to 2.48 eV) as the Si-doping in the samples increases. Other reports have observed and explained this observation as a decrease in donor–acceptor pairs, where the oxygen vacancy (V_O) donors are reduced^{7,13,29,32}. The same phenomenon has been seen in other reports for Sn-doped β -Ga₂O₃, which measured PL before and after annealing, and showed a dominant UV emission around 380 nm (3.26 eV) for both cases^{33–35}. Quenching of the UV emission, relative to the blue/green after annealing, was seen resulting from an increase in non-radiative recombination (conductivity), which was suggested to be due to a change in the formation of oxygen vacancies and gallium vacancy-oxygen vacancy complexes^{33,35}.

(-201) Orientation series. The three (-201) oriented samples in this series show several differences even though all the samples are UID β -Ga₂O₃. Depicted in Fig. 3 is the polarized PL of (-201) UID β -Ga₂O₃ film grown on Fe-doped β -Ga₂O₃, a (-201) UID β -Ga₂O₃ bulk crystal, and a (-201) UID β -Ga₂O₃ film grown on sapphire, all excited above and below bandgap. The bulk crystal and the β -Ga₂O₃ film grown on β -Ga₂O₃ both show polarization dependence of emission with weak dependence above (235 nm or 5.27 eV) and intense dependence below (267 nm or 3.22 eV) bandgap. But the β -Ga₂O₃ film grown on the sapphire substrate shows no polarization no matter what excitation is used, as seen in Fig. 3. This is attributed to rotational domains generated in the growth process for β -Ga₂O₃ films when grown on sapphire, which is the development of a twofold crystal on a threefold substrate as described by Ghadbeigi et al. as well as in several other studies^{36–38}. As such, polarization dependence is not expected, and the PL at each polarization should be an average arising from the rotationally misaligned crystalline domains.

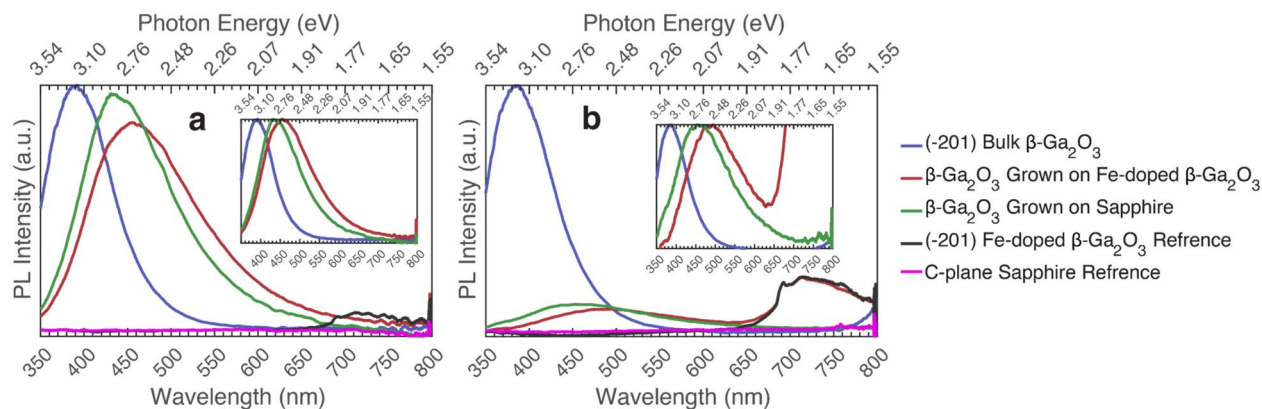


Figure 4. Photoluminescence comparison (taken at max polarization) of β - Ga_2O_3 grown on different substrates. Insets show the same data but normalized to the peak values. **(a)** Excited at 235 nm (5.27 eV), **(b)** Excited at 267 nm (4.64 eV).

Depicted in Fig. 4 is a PL comparison of all the (-201) UID β - Ga_2O_3 samples excited above and below the bandgap. As seen, the PL intensity from all samples is comparable above (235 nm or 5.27 eV) bandgap; but, below (267 nm or 4.64 eV) bandgap, the intensity of the epitaxial films diminishes considerably compared to the bulk sample. Furthermore, the bulk sample shows a dominant UV peak around 390 nm (3.18 eV) both above and below the bandgap. However, the β - Ga_2O_3 films grown on β - Ga_2O_3 and on sapphire show a dominant blue emission around 460 nm (2.7 eV) and 430 nm (2.88 eV) above and below bandgap, respectively. Similar observations were made in other reports for β - Ga_2O_3 grown on sapphire showing a dominant emission around 440 nm (2.82 eV)^{30,39,40}. The difference in dominant emission between samples of this series is likely due to extended defects ruling the emission of the PL found in epitaxial films. The studied bulk β - Ga_2O_3 crystals are assumed to have a small density of extended defects compared to an epitaxially grown film due to being a single crystal. Furthermore, note that the PL emission for the bulk β - Ga_2O_3 and the Si-doped series both have a dominant UV peak, even though the Si-doped series was epitaxially grown and had varying amounts of point defects in the samples, which did not cause a shift in the dominant UV peak. As previously shown, β - Ga_2O_3 grown on (010) β - Ga_2O_3 produces a homogeneous film with no stacking faults or extended defects^{30,31}.

On the other hand, both the epitaxial films in the (-201) oriented series are riddled with extended defects, as has been documented in several reports. Along with multiple reports, including Ghadbeigi et al. which showed rotational domains^{36–39}, TEM images of (-201) β - Ga_2O_3 grown on sapphire revealed multiple extended defects in these types of samples^{31,37–39,41–44}. Furthermore, Eisner et al. studied a similarly MOVPE grown sample like the β - Ga_2O_3 film grown on (-201) Fe-doped β - Ga_2O_3 . Using TEM, they showed that the film quality was poor and exhibited multiple extended defects throughout the sample⁴⁵. Additionally, the Si-doped series has comparable growth conditions to the (-201) β - Ga_2O_3 film grown on a differently oriented β - Ga_2O_3 substrate, suggesting that growth conditions that could change the number of a specific type of point defect in the sample could be ruled out. The only difference between the Si-doped series and (-201) grown on Ga_2O_3 is that β - Ga_2O_3 grown on (010) β - Ga_2O_3 yields a homogeneous film while β - Ga_2O_3 grown on (-201) β - Ga_2O_3 yields a poor-quality film riddled with extended defects. Thus, we hypothesize a strong correlation between the dominant blue peak seen in (-201) β - Ga_2O_3 film samples and extended defects.

AGO series. Shown in Fig. 5 is the polarized PL of four (010) oriented $(\text{Al}_x\text{Ga}_{1-x})_2\text{O}_3$, of varying Al concentration grown on Fe-doped β - Ga_2O_3 samples, excited above and below the bandgap and is further compared to a (100) oriented bulk 10% AGO sample. The AGO films show several differences compared to the UID β - Ga_2O_3 film and bulk 10% AGO crystal. The UID β - Ga_2O_3 film and bulk AGO crystal have a stronger polarization dependence than the two AGO film samples. The AGO films have a smaller polarization difference between the maximum and minimum polarization states.

Furthermore, there is a shift in the dominant peak as the polarization changes for the 25% AGO sample. This polarization shift could be due to aluminum atoms preferring the tetrahedral sites within the monoclinic structure of β - Ga_2O_3 due to the atoms smaller size⁴⁶. This could result in more types of one defect seen at the 0-degree polarization while a second defect rules the 90-degree orientation. But this is not seen in the bulk AGO crystal or 10% AGO film, which would be expected to show a similar polarization dependence shift in PL if this were the case. Thus, more studies are required to determine the cause of this shift.

Seen in Fig. 6 is a comparison of PL for AGO films with different Al concentrations grown on (010) Fe-doped β - Ga_2O_3 , excited above and below the bandgap. There is a clear difference in intensity between UID β - Ga_2O_3 and all AGO samples below (267 nm or 4.64 eV) and above (235 nm or 5.27 eV) bandgap. This difference in intensity could be due to the aluminum generating more non-radiative recombination paths, quenching of radiative paths, or due to an increase in the radiative recombination lifetime. Furthermore, the intensity is greater for 25% AGO than 10% AGO when excited at 235 (5.27 eV) nm, as seen in Fig. 6a. This is due to the shift in bandgap that occurs in alloyed materials. Using Vegard's law with a bowing parameter of 1.3^{47–49}, β - Ga_2O_3 has

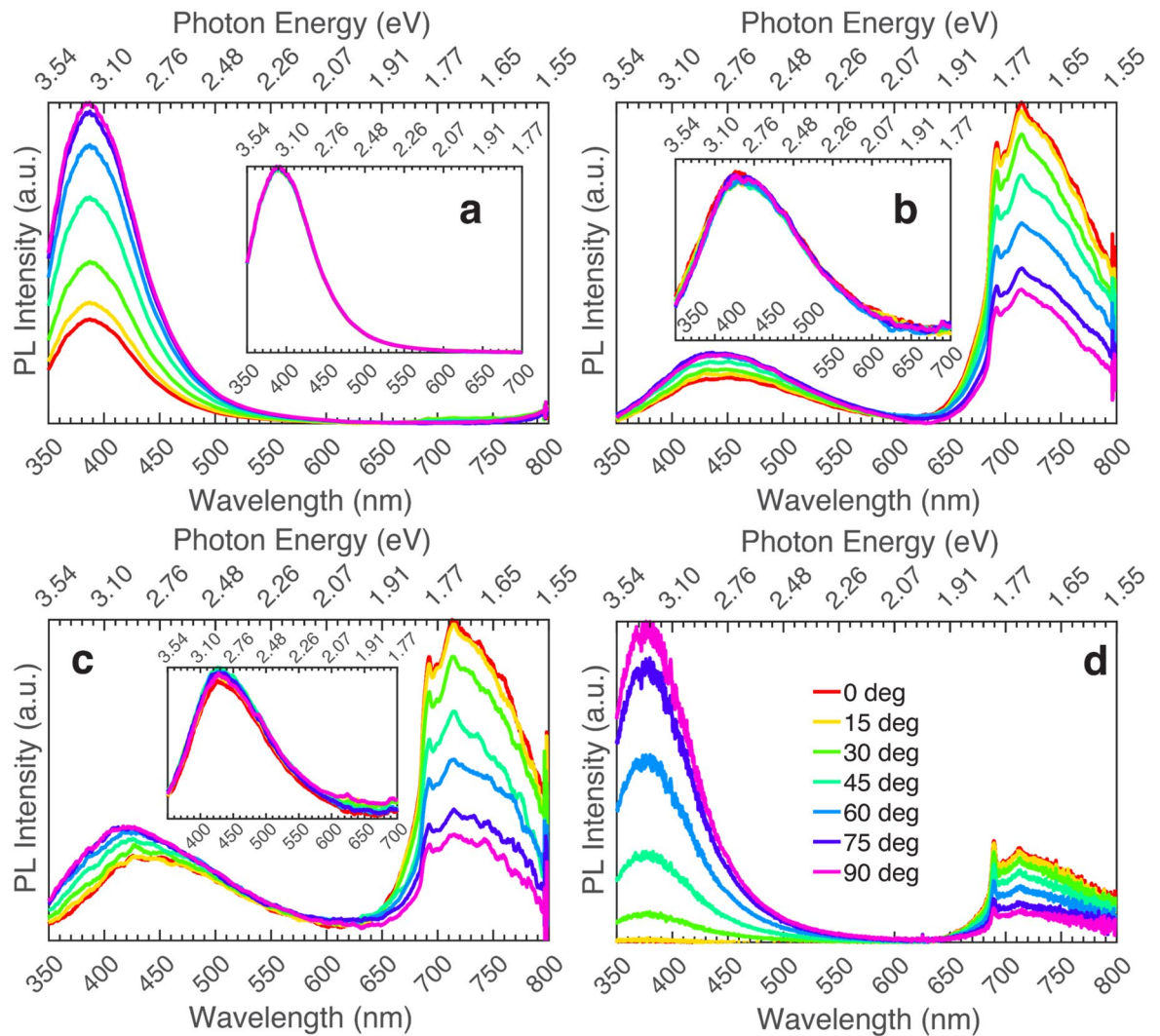


Figure 5. Polarized photoluminescence of different concentrations of AGO grown on (010) Fe-doped β -Ga₂O₃ excited at 254 nm (4.88 eV) except for (d). Insets show data for the same samples but excited at 235 nm (5.27 eV). (a) UID β -Ga₂O₃ grown on (010) Fe-doped β -Ga₂O₃, (b) 10% AGO grown on (010) Fe-doped β -Ga₂O₃, (c) 25% AGO grown on (010) Fe-doped β -Ga₂O₃, (d) 10% (100) bulk AGO excited at 235 nm (5.27 eV).

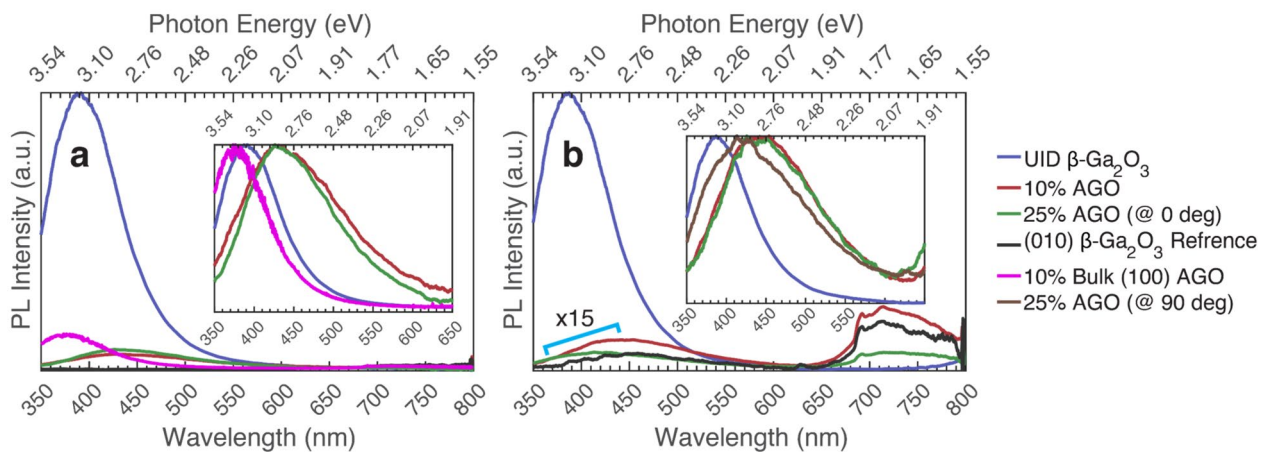


Figure 6. Photoluminescence comparison (taken at max polarization unless stated) of different concentrations of AGO grown on (010) Fe-doped β -Ga₂O₃ as well as compared to a 10% bulk (100) AGO sample. Inset depicts the same plot normalized. (a) Excited at 235 nm (5.27 eV), (b) Excited at 254 nm (4.88 eV).

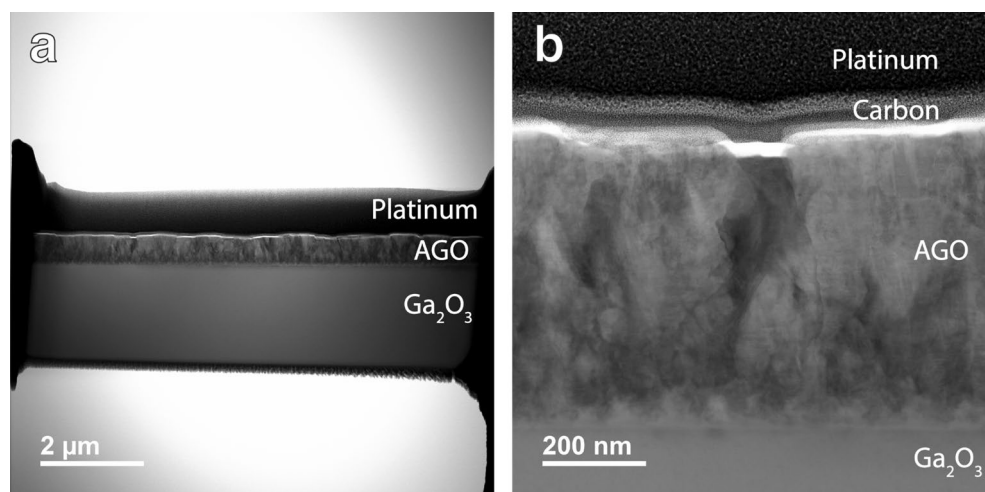


Figure 7. Darkfield STEM of 25% AGO grown on (010) Fe-doped β -Ga₂O₃. (a) Overview of the sample, (b) Section zoomed in.

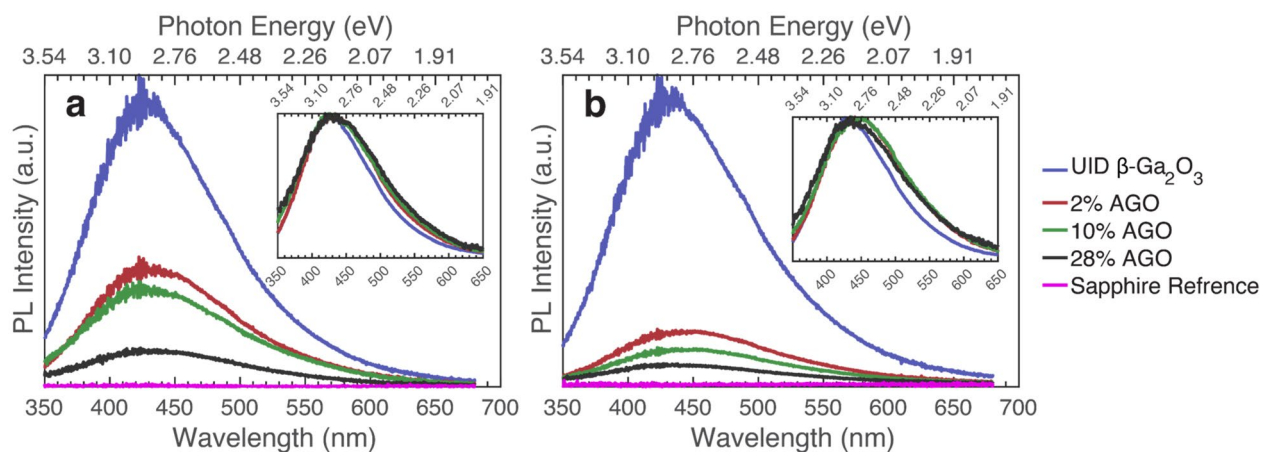


Figure 8. Photoluminescence comparison of different concentrations of AGO grown on c-plane sapphire. Inset depicts the same data smoothed using a 5-point moving average and then normalized to the peak value. (a) Excited at 236 nm (5.25 eV), (b) Excited at 254 nm (4.88 eV).

a bandgap around 258.3 nm (4.8 eV), 10% AGO has a bandgap around 248 nm (5.0 eV), and 25% AGO has a bandgap around 234 nm (5.3 eV). On the other hand, the excitation used for Fig. 6a is 235 nm (5.27 eV). The maximum PL intensity for a sample is expected to be seen around its bandgap. At higher excitation energies, a strong absorption coefficient inhibits light from penetrating deep into the sample, so a higher percentage of photocarriers diffuse and recombine, causing lower radiative recombination. At lower excitation energies below the bandgap, the effects of bulk recombination and small optical thickness are accentuated, so there is less radiative recombination³⁶. Since the excitation of 235 nm (5.27 eV) is closer to the bandgap of 25% AGO, there is a higher PL intensity for 25% AGO than for 10% AGO at that excitation. For the same reason, at an excitation of 254 nm (4.88 eV), as shown in Fig. 6b, a larger PL intensity for 10% AGO than 25% AGO is observed.

There is also a clear shift between the dominant emission peak between samples. The UID β -Ga₂O₃ film shows a dominant UV emission at 390 nm (3.18 eV), as for the Si-doped series and the (-201) bulk β -Ga₂O₃ crystal. The bulk AGO crystal also has a dominant UV emission, but around 380 nm (3.26 eV). On the other hand, the epitaxial AGO films have a dominant blue emission around 430 nm (2.88 eV) and are consistent with the (-201) oriented heteroepitaxial film grown on sapphire. This can again be explained by the extended defects found throughout the sample.

TEM was done on the 25% AGO film grown on (010) oriented Fe-doped β -Ga₂O₃ using the JEOL JEM 2800 Scanning Transmission Electron Microscope. The dark field image is shown in Fig. 7. Even though the films were grown on (010) oriented β -Ga₂O₃ and tend to be homogeneous, the AGO films analyzed here, which were produced on the same substrate, show many extended defects as seen in the Fig. 7 Scanning TEM (STEM) image. This is likely caused by the high growth rate used to make the films thicker, which caused the epitaxy to break

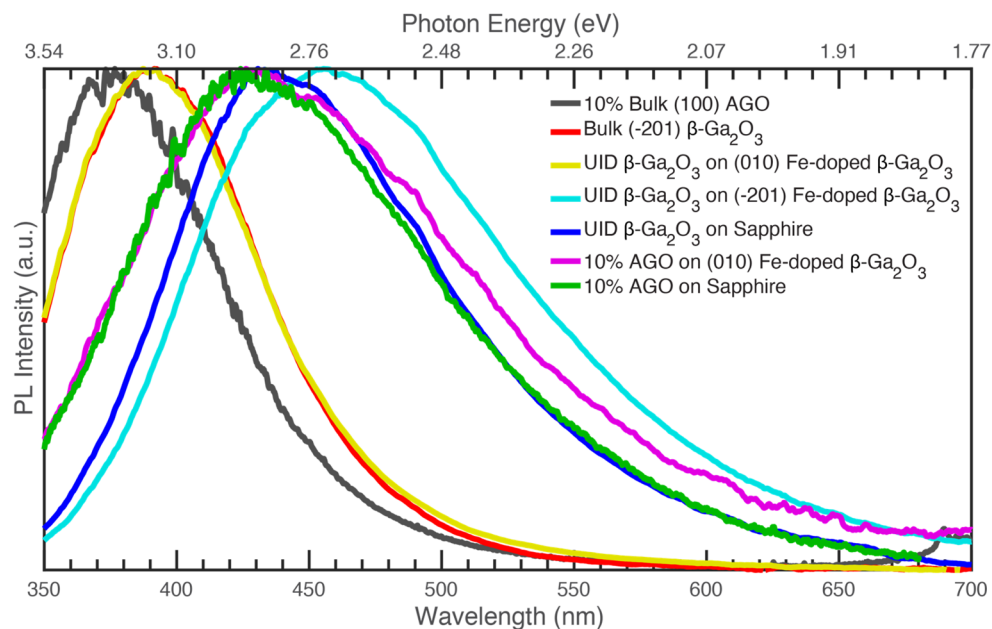


Figure 9. Normalized photoluminescence (taken at max polarization) comparison of all samples previously discussed excited at 235 nm (5.27 eV). The AGO grown on the sapphire sample was excited at 236 nm (5.25 eV), and the data were smoothed using a 5-point moving average before being normalized to the peak intensity.

down. Furthermore, there is no difference between the 10% AGO and 25% AGO dominant blue PL emission, even though the number of point defects has changed between samples (and some of the growth conditions to accommodate for the desired aluminum concentration). There is a decrease in broadening from 10% AGO to 25% AGO, but this broad PL resembles that of the other defective samples. Again, the only real difference between UV dominant and blue dominant samples is that the blue dominant samples are riddled with extended defects, further revealing a correlation between a blue-centered PL spectrum and a large density of extended defects.

Lastly, the four samples in the AGO series grown on sapphire show consistent PL results with what has previously been seen. This is shown in Fig. 8, where the PL for AGO samples grown on sapphire with different Al concentrations are shown (excitation above and below bandgap). The series contains (-201) oriented 0%, 2%, 10%, and 28% AGO films grown on sapphire. No polarization dependences at any excitation were observed due to rotational domains in the (-201) oriented β -Ga₂O₃ film grown on sapphire. The dominant emission is in the blue, with the emission peak occurring at around 430 nm (2.88 eV). This is the same for all samples in this series. This is also consistent with the position of the dominant peak seen for the AGO films grown on (010) β -Ga₂O₃ and the (-201) oriented heteroepitaxial film grown on sapphire. Again, this is likely due to extended defects seen throughout the film, developed from a combination of the poor-quality film an alloy generates as well as a poor-quality film that is caused by growing on sapphire. This correlates with TEM images showing poor AGO films grown on sapphire discussed in previous papers^{42,50–53}. Other observations seen in Fig. 8, which compares all the AGO films grown on sapphire, include the intensity decreasing with increasing aluminum concentration. This could be due to an increase in the electron–phonon coupling, as discussed for the other AGO samples. This could also explain why UID β -Ga₂O₃ PL does not extend so far into the blue and green emission as the AGO samples do. Another explanation could be due to the appearance of aluminum atoms creating new recombination paths that generate more blue and green emissions, though more study is necessary to determine the specific processes.

Conclusions

Si-doped β -Ga₂O₃ grown on (010) β -Ga₂O₃ yields homogeneous crystalline films with a low density of extended defects and a dominant UV emission in PL. This is the same as what is seen for bulk crystals, including (-201) β -Ga₂O₃. Heteroepitaxial and homoepitaxial (-201) β -Ga₂O₃ films show consistent PL features with dominant blue emission and small UV luminescence. The films' poor quality is likely the reason for this shift in the dominant emission, as observed when comparing UID films grown on (010) and (-201) bulk β -Ga₂O₃ crystals with comparable growth conditions. AGO for both homoepitaxial and heteroepitaxial samples also shows consistent blue centered PL with no UV emission observed. All these samples show extended defects throughout a poor-quality film. As such, we have hypothesized that extended defects have an essential role in the PL emission of β -Ga₂O₃ and AGO films. Homogeneous films with no extended defects or stacking faults and bulk crystals will yield a UV dominant PL emission. Samples of poor film quality that have stacking faults and extended defects will have a dominant blue PL emission. This is clearly shown in Fig. 9, which compares representative samples chosen from all the series previously discussed (excited at 235 nm or 5.27 eV). As seen, bulk crystals (both β -Ga₂O₃ and β -Al_{0.2}Ga_{1.8}O₃, i.e., 10% AGO) and β -Ga₂O₃ films grown on (010) β -Ga₂O₃ all have a similar dominant UV peak PL signature likely because all samples are of good quality with minimal extended defects.

On the other hand, β -Ga₂O₃ films grown on sapphire, AGO films grown on (010) β -Ga₂O₃, and AGO films grown on sapphire all show the same dominant blue emission, even with differing defects and growth conditions. The only fundamental similarity for those samples is that all have proven to have poor quality films with large densities of extended defects, which do not necessarily have the same associated defect states as isolated point defects. β -Ga₂O₃ films grown on sapphire have extended defects developing from at least rotational domains. And films grown on (-201) β -Ga₂O₃ show an even more significant shift for the dominant blue emission. Again, the major difference between β -Ga₂O₃ films grown on (-201) β -Ga₂O₃ and β -Ga₂O₃ films grown on (010) β -Ga₂O₃ is that the (-201) β -Ga₂O₃ film exhibits a large density of extended defects which could arise from a chain of point defects or dislocations, stacking faults, interfaces, etc. And, it can be difficult to pinpoint the exact mechanisms as any defect considered can result in a very wide luminescence band, even near 0 K. That said, follow-up studies are needed to better understand the specific processes involved in these samples to understand the broadening and shifts seen in Fig. 9 and conclusively determine what recombination processes are dominant within the different series of samples.

Received: 8 December 2021; Accepted: 15 February 2022

Published online: 25 February 2022

References

1. Pearton, S. *et al.* A review of Ga₂O₃ materials, processing, and devices. *Appl. Phys. Rev.* **5**, 011301 (2018).
2. Alkauskas, A., McCluskey, M. D. & Van de Walle, C. G. Tutorial: Defects in semiconductors—Combining experiment and theory. *J. Appl. Phys.* **119**, 181 (2016).
3. Zhang, J. Applications of huang-rhys theory in semiconductor optical spectroscopy. *J. Semicond.* **40**, 091102 (2019).
4. Li, S. L. & Truhlar, D. G. Franck-Condon models for simulating the band shape of electronic absorption spectra. *J. Chem. Theory Comput.* **13**, 2823–2830 (2017).
5. Herbert, W. C., Minnier, H. B. & Brown, J. J. Jr. Self-activated luminescence of β -Ga₂O₃. *J. Electrochem. Soc. Solid State Sci.* **116**, 1019–1021 (1969).
6. Tomm, Y., Reiche, P., Klimm, D. & Fukuda, T. Czochralski grown Ga₂O₃ crystals. *J. Cryst. Growth.* **220**, 510–514 (2000).
7. Shimamura, K., Villora, E. G., Ujii, T. & Aoki, K. Excitation and photoluminescence of pure and Si-doped β -Ga₂O₃ single crystals. *Appl. Phys. Lett.* **92**, 201914 (2008).
8. Wakai, H., Sinya, Y. & Yamanaka, A. Effect of Cr³⁺ ions on Optical Properties in β -Ga₂O₃ Semiconductor. *Phys. Status Solidi C*. **8**, 537–539 (2011).
9. Yamaga, M. *et al.* Polarization of optical spectra in transparent conductive oxide β -Ga₂O₃. *Phys. Status Solidi C*. **8**, 2621–2624 (2011).
10. Onuma, T. *et al.* Correlation between blue luminescence intensity and resistivity in β -Ga₂O₃ single crystals. *Appl. Phys. Lett.* **103**, 041910 (2013).
11. Yamaoka, S. & Nakayama, M. Evidence for formation of self-trapped excitons in a β -Ga₂O₃ single crystal. *Phys. Status Solidi C*. **13**, 93–96 (2016).
12. Bordun, O. M., Bordun, B. O., Kukharsky, I. Y. & Medvid, I. I. Photoluminescence properties of β -Ga₂O₃ thin films produced by ion-plasma sputtering. *J. Appl. Spectrosc.* **84**, 46–51 (2017).
13. Oda, H., Kimura, N., Yasukawa, D., Wakai, H. & Yamanaka, A. Time-resolved spectroscopy of luminescence in a wide gap Si-doped β -Ga₂O₃. *Phys. Status Solidi A*. **214**, 1600670 (2017).
14. Ho, Q. D., Frauenheim, T. & Deák, P. Origin of photoluminescence in β -Ga₂O₃. *Appl. Phys. Rev. B*. **97**, 115163 (2018).
15. Huynh, T. T., Lem, L. L. C., Kuramata, A., Phillips, M. R. & Ton-That, C. Kinetics of charge carrier recombination in β -Ga₂O₃ crystals. *Phys. Rev. Mater.* **2**, 105203 (2018).
16. Liu, C. *et al.* Irradiation effects on the structural and optical properties of single crystal β -Ga₂O₃. *Semicond. Sci. Technol.* **33**, 095022 (2018).
17. Wang, Y. *et al.* Incident wavelength and polarization dependence of spectral shifts in β -Ga₂O₃ UV photoluminescence. *Sci. Rep.* **8**, 18075 (2018).
18. Berencén, Y. *et al.* Structural and optical properties of pulsed-laser deposited crystalline β -Ga₂O₃ thin films on silicon. *Semicond. Sci. Technol.* **34**, 035001 (2019).
19. Cui, H. *et al.* Analysis on the electronic trap of β -Ga₂O₃ single crystal. *J. Mater. Sci.* **54**, 12643–12649 (2019).
20. Hany, I. *et al.* Low temperature cathodoluminescence study of Fe-doped β -Ga₂O₃. *Mater. Lett.* **257**, 126744 (2019).
21. Huso, J., McCluskey, M. D., Yu, Y., Islam, Md. M. & Selim, F. Localized UV emitters on the surface of β -Ga₂O₃. *Sci. Rep.* **10**, 21022 (2020).
22. Cho, J. B. *et al.* Highly asymmetric optical properties of β -Ga₂O₃ as probed by linear and nonlinear optical excitation spectroscopy. *J. Phys. Chem. C*. **125**, 1432–1440 (2021).
23. Jesenovec, J. *et al.* Gallium vacancy formation in oxygen annealed β -Ga₂O₃. *J. of Appl. Phys.* **129**, 245701 (2021).
24. Zhang, N. *et al.* Anisotropic luminescence and third-order electric susceptibility of Mg-doped gallium oxide under the half-bandgap edge. *Opt. Express*. **29**, 18587–18600 (2021).
25. Jesenovec, J., Dutton, B., Stone-Weiss, N., Saleh, M. & McCloy, J. S. Alloyed (Al_xGa_{1-x})₂O₃ Bulk Czochralski Single and Polycrystals with High Al Concentration (x = 0.5, 0.33, 0.1). Submitted manuscript (2021).
26. Bhattacharyya, A. *et al.* Low temperature homoepitaxy of (010) β -Ga₂O₃ by metalorganic vapor phase epitaxy: Expanding the growth window. *Appl. Phys. Lett.* **117**, 142102 (2020).
27. Sun, R., Ooi, Y. K., Dickens, P. T., Lynn, K. G. & Scarpulla, M. A. On the origin of red luminescence from iron-doped β -Ga₂O₃ bulk crystals. *Appl. Phys. Lett.* **117**, 052101 (2020).
28. Luchechko, A., Vasylytsiv, V., Kostyk, L., Tsvetkova, O. & Pavlyk, B. Thermally stimulated luminescence and conductivity of β -Ga₂O₃ crystals. *J. Nano-Electron. Phys.* **11**, 03035 (2019).
29. Onuma, T. *et al.* Modeling and interpretation of UV and blue luminescence intensity in β -Ga₂O₃ by silicon and nitrogen doping. *J. Appl. Phys.* **124**, 075103 (2018).
30. Rafique, S. *et al.* Homoepitaxial growth of β -Ga₂O₃ thin films by low pressure chemical vapor deposition. *Appl. Phys. Lett.* **108**, 182105 (2016).
31. An, Y. *et al.* Epitaxial growth of β -Ga₂O₃ thin films on Ga₂O₃ and Al₂O₃ substrates by using pulsed laser deposition. *J. Adv. Dielect.* **9**, 1950032 (2019).
32. Kucukgok, B., *et al.* Optical and structural properties of Si doped β -Ga₂O₃ (010) thin films homoepitaxially grown by halide vapor phase epitaxy. physics.app-ph. arXiv: <https://arxiv.org/abs/1906.09306> (2019).

33. Ohira, S. *et al.* Characterization of transparent and conducting Sn-doped β -Ga₂O₃ single crystal after annealing. *Thin Solid Films* **516**, 5763–5767 (2008).
34. Naresch-Kumar, G. *et al.* Origin of red emission in β -Ga₂O₃ analyzed by cathodoluminescence and photoluminescence spectroscopy. *Phys. Status Solidi B* **258**, 200465 (2021).
35. Sun, R. *et al.* Oxygen annealing induced changes in defects within β -Ga₂O₃ epitaxial films measured using photoluminescence. *J. Phys. D Appl. Phys.* **54**, 174004 (2021).
36. Ghadbeigi, L. *et al.* Optical characterization of gallium oxide α and β polymorph thin-films grown on c-plane sapphire. *J. Electr. Mater.* **50**, 2990–2998 (2021).
37. Schewski, R. *et al.* Epitaxial stabilization of pseudomorphic α -Ga₂O₃ on sapphire (0001). *Appl. Phys. Express* **8**, 011101 (2015).
38. Rafique, S. *et al.* Towards high-mobility heteroepitaxial β -Ga₂O₃ on sapphire—Dependence on the substrate off-axis angle. *Phys. Status Solidi A* **215**, 1700467 (2018).
39. Feng, B. *et al.* Investigation of β -Ga₂O₃ film grown mechanism on c-plane sapphire substrate by ozone molecular beam epitaxy. *Phys. Status Solidi A* **218**, 200457 (2021).
40. Dong, L., Jia, R., Xin, B. & Zhang, Y. Effects of post-annealing temperature and oxygen concentration during sputtering on the structural and optical properties of β -Ga₂O₃ films. *J. Vac. Sci. Technol. A* **34**, 060602 (2016).
41. Nakagomi, S. & Kokubun, Y. Cross-sectional TEM imaging of β -Ga₂O₃ thin films formed on c-plane and a-plane sapphire substrates. *Phys. Status Solidi A* **210**, 1738–1744 (2013).
42. Song, Y. *et al.* Thermal conductivity of β -phase Ga₂O₃ and (Al_xGa_{1-x})₂O₃ heteroepitaxial thin films. *ACS Appl. Mater. Interfaces* **13**, 38477–38490 (2021).
43. Gogova, D., Schmidbauer, M. & Kwasniewski, A. Homo- and heteroepitaxial growth of Sn-doped β -Ga₂O₃ layers by MOVPE. *CrystEngComm* **17**, 6744–6752 (2015).
44. Gogova, D. Structural properties of Si-doped β -Ga₂O₃ layers grown by MOVPE. *J. Cryst. Growth* **401**, 665–669 (2014).
45. Eisner, B. A., Ranga, P., Bhattacharyya, A., Krishnamoorthy, S. & Scarpulla, M. A. Compensation in (01) homoepitaxial β -Ga₂O₃ thin films grown by metalorganic vapor-phase epitaxy. *J. Appl. Phys.* **128**, 195703 (2020).
46. Cook, D. S. *et al.* Synthesis and polymorphism of mixed aluminum-gallium oxides. *Inorg. Chem.* **59**, 3805–3816 (2020).
47. Li, J. *et al.* Identification and modulation of electronic band structures of single-phase β -(Al_xGa_{1-x})₂O₃ alloys grown by laser molecular beam epitaxy. *Appl. Phys. Lett.* **113**, 041901 (2018).
48. Wang, T., Li, W., Ni, C. & Janotti, A. Band gap and band offset of Ga₂O₃ and (Al_xGa_{1-x})₂O₃ alloys. *Phys. Rev. Appl.* **10**, 011003 (2018).
49. Peelers, H., Varley, J. B., Speck, J. S. & Van de Walle, C. G. Structural and electronic properties of Ga₂O₃-Al₂O₃ alloys. *Appl. Phys. Lett.* **112**, 242101 (2018).
50. Yuan, S. H., Ou, S. L., Huang, S. Y. & Wu, D. S. Enhanced deep-ultraviolet responsivity in aluminum-gallium oxide photodetectors via structure deformation by high-oxygen-pressure pulsed laser deposition. *ACS Appl. Mater. Interfaces* **11**, 17563–17569 (2019).
51. Liao, C. H., Li, K. H., Torres-Castanedo, C. G., Zhang, G. & Li, X. β -phase (Al_xGa_{1-x})₂O₃ thin film with Al composition more than 70%. arXiv: Appl. Phys. <https://arxiv.org/abs/2005.05799> (2020).
52. Hassa, A. *et al.* Control of phase formation of (Al_xGa_{1-x})₂O₃ thin films on c-plane Al₂O₃. *J. Phys. D: Appl. Phys.* **53**, 485105 (2020).
53. Jinno, R. *et al.* Crystal orientation dictated epitaxy of ultrawide-bandgap 5.4- to 8.6-eV α -(AlGa)₂O₃ on m-plane sapphire. *Sci. Adv.* **7**, eabd5891 (2021).

Acknowledgements

This material is based upon work supported by the Air Force Office of Scientific Research under award number FA9550-21-1-0507 (program manager: Dr. Ali Sayir). Any opinions, findings, and conclusions, or recommendations expressed in this material are those of the author(s) and do not necessarily reflect the views of the United States Air Force. This work made use of the University of Utah USTAR shared facilities supported, in part, by the MRSEC Program of NSF under Award No. DMR-1121252.

Author contributions

B.S.-R. and M.A.S. designed this project. J.J. grew and characterized the bulk AGO sample with J.S.M. guidance. P.R. grew all the epitaxial samples and carried out XRD measurements for epitaxially grown AGO calculating % of Al with S.K. guidance. J.C. carried out PL and TEM characterization and wrote the draft of this manuscript. This manuscript was written through contributions of all authors. All authors have given approval to the final version of this manuscript.

Competing interests

The authors declare no competing interests.

Additional information

Supplementary Information The online version contains supplementary material available at <https://doi.org/10.1038/s41598-022-07242-z>.

Correspondence and requests for materials should be addressed to B.S.-R.

Reprints and permissions information is available at www.nature.com/reprints.

Publisher's note Springer Nature remains neutral with regard to jurisdictional claims in published maps and institutional affiliations.



Open Access This article is licensed under a Creative Commons Attribution 4.0 International License, which permits use, sharing, adaptation, distribution and reproduction in any medium or format, as long as you give appropriate credit to the original author(s) and the source, provide a link to the Creative Commons licence, and indicate if changes were made. The images or other third party material in this article are included in the article's Creative Commons licence, unless indicated otherwise in a credit line to the material. If material is not included in the article's Creative Commons licence and your intended use is not permitted by statutory regulation or exceeds the permitted use, you will need to obtain permission directly from the copyright holder. To view a copy of this licence, visit <http://creativecommons.org/licenses/by/4.0/>.

© The Author(s) 2022